

# Electrochemical investigation of a rotationally flexible bibenzimidazole di-iron complex

Markus Nilsson<sup>a,1</sup>, Pablo G. Porta<sup>b</sup>, Dieter Sorsche<sup>b</sup>, Elisabet Ahlberg<sup>a</sup>, Michael Busch<sup>c,d,\*</sup>

<sup>a</sup> Department of Chemistry and Molecular Biology, University of Gothenburg, Medicinaregatan 7B, 413 90 Gothenburg, Sweden

<sup>b</sup> Institute of Inorganic Chemistry I, Ulm University, Albert-Einstein-Allee 11, 89081 Ulm, Germany

<sup>c</sup> Department of Engineering Sciences and Mathematics, Applied Physics, Luleå University of Technology, 971 87 Luleå, Sweden

<sup>d</sup> Wallenberg Initiative Materials Science for Sustainability (WISE), Luleå University of Technology, 971 87 Luleå, Sweden

## ARTICLE INFO

### Keywords:

Diiron complexes  
Molecular electrochemistry  
Density functional theory

## ABSTRACT

Ligand systems used for electrochemical reductions commonly comprise single metal centres. This is opposed to complexes with two or more adjacent metals which are significantly less studied. In order to fill this gap a Fe dimer embedded into the 1,1',5,5',6,6'-hexamethyl-4,4'-bis(picolinimino)-2,2'-bibenzimidazole (<sup>Me</sup>bpbbi) ligand system is studied in the present work with focus on electrochemical properties in acetonitrile solution. A combination of cyclic voltammetry and density functional theory (DFT) reveals that the complex is present at least as an open, non-bridged, and a closed, ( $\mu$ -Cl)<sub>2</sub> bridged complex. Both forms possess very different redox properties and ligand exchange energetics. The presence of a stable reversible electron transfer couple for the non-bridged complex is promising for electrocatalytic reactions. Surprisingly, our calculations demonstrate that the iron ions essentially maintain their charge while the ligand accommodates the charges involved in the different redox steps.

## 1. Introduction

In homogeneous catalysis the choice of ligand system is often as important as the choice of active metal. This resulted in a myriad of ligand systems for chemical conversions. Examples of ligand systems range from very simple ligands like CO [1] to complex organic systems like porphyrin [2,3], phthalocyanine [4–6], pyridines [7–9] or phosphines [10–12]. Many of these ligands are also used in homogeneous electrocatalysis. However, their use under electrochemical conditions is often limited due to decomposition under applied potentials [13,14]. Accordingly, most electrochemical studies only consider a few selected ligands. Of these systems, porphyrins and phthalocyanines for reactions like CO<sub>2</sub> reduction [4,15–17] or epoxidations [18,19] and terpyridine systems for water oxidation [9,20,21] are most common.

Most systems investigated for electrocatalytic reductions are mononuclear. This is opposed to classical homogeneous catalysis, where binuclear systems have received increased attention over the last years [22–24]. Many of these catalysts mimic enzymes like the [FeFe] hydrogenases or the methane monooxygenases [25–27]. The ligands to construct these biomimetic catalysts possess, however, often a rigid

geometry which predetermines the distance between the two metal centres and thus, the level of cooperativity [22–24]. A possibility to avoid this limitation is the introduction of a flexible ligand framework. Such a system was introduced by Muller et al. 30 years ago [28]. The ligand consists of two symmetric picolinimino-benzimidazole frameworks which are connected through a C–C single bond. This allows for free rotation (Fig. 1). The original complex was based on a Cu dimer and constructed to represent a model of the oxygen transport enzyme haemocyanine. Recently we added an Fe dimer coordinated into this 1,1',5,5',6,6'-hexamethyl-4,4'-bis(picolinimino)-2,2'-bibenzimidazole (<sup>Me</sup>bpbbi) ligand system which was studied in detail through a combination of computational and experimental techniques [29]. According to our results, this complex can be present both in a closed, (Cl)<sub>2</sub> bridged and an open Cl terminated, non-bridged, form (Fig. 1). Both isomers are connected by a low barrier which enables interconversion between both species. The speciation is further complicated by the fact that minor changes such as a temperature decrease can trigger ligand exchange reactions whereby one or more Cl<sup>−</sup> are replaced by a solvent molecule. This complexity is also represented in the electrochemistry of the molecule. Preliminary measurements in the presence of LiCl suggest the

\* Corresponding author.

E-mail address: [michael.busch@ltu.se](mailto:michael.busch@ltu.se) (M. Busch).

<sup>1</sup> Present address: Department of Chemistry and Chemical Engineering, Chalmers University of Technology, Kemivägen 10, 412 96 Gothenburg, Sweden

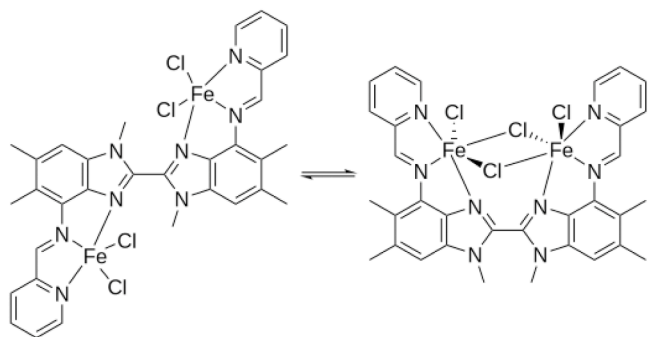


Fig. 1. Non-bridged and bridged isomers of the <sup>Me</sup>bpbpi based diiron complex.

presence of one reversible peak followed by a series of irreversible reduction reactions. Indeed, the presence of a reversible peak hints at the possibility to use this complex as an electrocatalyst but the complexity of the cyclic voltammetry (CV) measurements requires a more detailed analysis of its electrochemistry.

In what follows, we will present a detailed analysis of the complex's electrochemical behaviour using a combination of density functional theory (DFT) computations and CV. Our analysis suggests that the non-bridged complex is responsible for the reversible peak and that the irreversible peaks originate from the bridged complex. Thus, likely only the open form can be used for catalysis. All irreversible reaction steps are associated with the exchange of Cl<sup>-</sup> by solvent molecules which needs to be suppressed if the ligand is to be used as homogeneous electrocatalyst.

## 2. Experimental and computational details

### 2.1. Synthesis

1,1',5,5',6,6'-hexamethyl-4,4'-bis(picolinimino)-2,2'-bibenzimidazole (<sup>Me</sup>bpbpi) was synthesised through a five-step synthesis described by Muller et al [28]. In the first step of the synthesis 1,1',5,5',6,6'-hexamethyl-4,4'-bis(picolinimino)-2,2'-bibenzimidazole is formed through condensation of trichloroacetic acid with 4,5-dimethyl ortho phenylenediamine followed by an oxidation of the amino groups with H<sub>2</sub>SO<sub>4</sub>/HNO<sub>3</sub> to the corresponding nitro substituents to protect them from ethylation in the subsequent step. Methylation in the 1,1' positions was achieved with methyl iodide and followed by the reduction of the nitro groups to their corresponding amines using SnCl<sub>2</sub>/HCl. The final product was afforded through double condensation with 2-picolinecarbaldehyde. The Fe complex was obtained through coordination of FeCl<sub>2</sub> in dry tetrahydrofuran (THF) under a N<sub>2</sub> protective atmosphere. The reader is referred to reference [29] for a detailed description of the synthesis, reaction conditions, and used chemicals. All measurements were performed using the batch characterised in reference [29].

### 2.2. Electrochemistry

All electrochemical measurements presented in this work were performed in acetonitrile solution (≥99.9% and 99.999%) purchased from Honeywell and Sigma-Aldrich, respectively, using a supporting electrolyte of 0.1 M tetrabutylammonium tetrafluoroborate (NBu<sub>4</sub>BF<sub>4</sub>, 99%) purchased from Sigma-Aldrich. Samples were purged with nitrogen before measurements and kept under nitrogen atmosphere during experiments. Electrochemical measurements were carried out in a three-electrode cell using a glassy carbon working electrode (3 mm diameter), platinum mesh counter electrode, and a Ag/Ag<sup>+</sup> reference electrode (10 mM AgNO<sub>3</sub> and 0.1 M NBu<sub>4</sub>BF<sub>4</sub> in acetonitrile), *E* = 0.44 V vs. SHE [30]. Experiments were controlled using a Metrohm Autolab AUT72461 potentiostat (installed modules: ADC164, BIPOT, DAC164, FRA32M, pX1000, and SCAN250) with a PSGSTAT12/30 Differential Electrometer Amplifier dongle).

**Measurement Procedure.** Measurements were set up and run through the Nova version 2 software supplied by Metrohm. Measurement of the open circuit potential (OCP) was performed at the start of each measurement series, either until a stable value was reached  $dE/dt < 1 \mu\text{Vs}^{-1}$  or for a maximum of 300 s. This was followed by a single linear CV scan or a series of scans at different rates. Before each scan the cell was kept at the initial potential for 30 s. In the case of repeated scans, the OCP was applied for 100 s between each scan to re-establish equilibrium. In addition, rates were applied in the order: 0.1, 0.5, 0.02, 1.5, 0.2, 2.0, 0.05, and 1.0 V s<sup>-1</sup> to avoid correlation of effects caused by time and scan rate.

Early measurements revealed that results were affected by previous scans going to negative potentials of more than -0.5 V. It was however found that polishing the electrode surface before each measurement mitigated this effect. As a result, for all the voltammograms presented the electrode was polished before each series of scans, i.e. before each single scan and at the start of each series of scans with varying rates.

**Thermochemistry.** Density functional theory (DFT) calculations were performed using Gaussian 16 Rev. C.01 [31]. The M06-L functional [32] was used to compute the energetics of the transition metal complexes.

Calculations were performed in two parts; for geometry optimisations and frequency calculations the def2-SVP [33] basis set and PCM [34,35] solvation model was used, while for single-point calculations the def2-TZVP [33] basis set and SMD [36] solvation model were used. Gibbs Free energy corrections were taken from a vibrational analysis at the M06-L/Def2-SVP/PCM level of theory used for geometry optimisation. All structures were assumed converged if the following convergence criteria were fulfilled: Maximum force  $F_{\text{max}} = 4.5 \times 10^{-4}$  HaBohr<sup>-1</sup>; RMS force  $F_{\text{RMS}} = 3.00 \times 10^{-4}$  HaBohr<sup>-1</sup>; maximum displacement:  $1.80 \times 10^{-3}$  Bohr; RMS displacement:  $1.20 \times 10^{-3}$  Bohr. Additionally, we verified that the obtained structure truly corresponds to a local minimum by ensuring that all imaginary modes are below 100i cm<sup>-1</sup>.

Solvation energies obtained using implicit solvation models, such as PCM and SMD used in this work, are known to be unreliable, especially for charged species [37–39]. In this work this mainly affects the free chloride ion. To minimise this error, the experimental solvation energy for Cl<sup>-</sup> in acetonitrile of -2.80 eV [40] was used to obtain the energy of the solvated species from the calculated Gibbs free energy of the species in gas phase. In addition, a standard state of 1 bar at 298.15 K was used in the calculations which means that the calculated energy must be converted to a solvated standard state (1 M, 298.15 K) through addition of the correction factor 82 meV [41]. Finally, the Gibbs free energy, *G*, at experimental conditions can be computed through Eq. (2):

$$G = G^0 + RT \ln \left( \frac{[\text{Cl}^-]}{[\text{Cl}^-]^0} \right) \quad (2)$$

where *G*<sup>0</sup> is the Gibbs free energy at the solvated standard state (1 M, 298.15 K), *R* the general gas constant, *T* the temperature and [Cl<sup>-</sup>] and [Cl<sup>-</sup>]<sup>0</sup> the chloride concentration under experimental (10 μM) and standard conditions (1 M), respectively.

A similar correction was performed for solvated acetonitrile in acetonitrile solvent. However, since solvation of a gas molecule in the same liquid is just condensation, the solvation energy can be approximated from the enthalpy of vaporisation  $\Delta H_{\text{vap}}(T_{\text{vap}})$  and the heat capacity under constant pressure *C*<sub>p</sub>. Using *C*<sub>p</sub> = 0.95 meV·mol<sup>-1</sup>·K<sup>-1</sup>, [42]  $\Delta H_{\text{vap}}(T_{\text{vap}}) = 0.31$  eV [42], and *T*<sub>vap</sub> = 81.7 °C at *T* = 25 °C [42],  $\Delta G_{\text{solv}} = 0.36$  eV.

Presented potentials, both experimental and computational, are given relative to the Ag/Ag<sup>+</sup> reference electrode. Electron transfer potentials versus the standard hydrogen electrode (SHE) in water were computed using an effective absolute potential and converted using the corresponding reference potential *E*<sub>ref</sub>(Ag/Ag<sup>+</sup>) = 0.44 V versus the computational aqueous SHE [43]. The absolute potential in water was

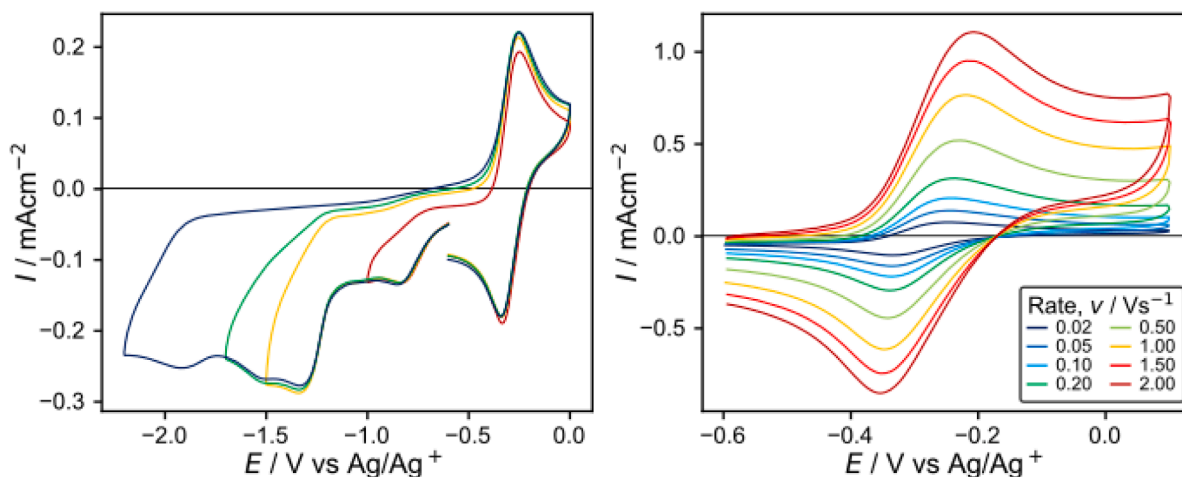


**Fig. 2.** a) Cyclic voltammograms for a complex solution (1 mM complex, 0.1 M NBu<sub>4</sub>BF<sub>4</sub> in acetonitrile) with varying vertex potentials at a scan rate of 0.1 Vs<sup>-1</sup>. b) Cyclic voltammograms in a restricted potentials range showing the reversible redox couple at different sweep rates from 0.02 to 2 Vs<sup>-1</sup>. The heterogeneous rate constant was determined to 0.1 cm s<sup>-1</sup> and the diffusion coefficient to 5·10<sup>-6</sup> cm<sup>2</sup>s<sup>-1</sup>.

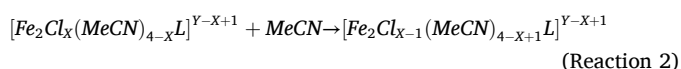
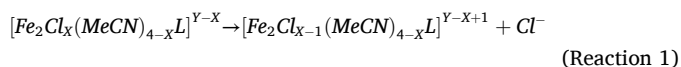
computed using the formic acid / formate acid base couple ( $pK_a = 3.75$  [44]), giving a value of 4.02 V.

Activation energies were estimated using the method suggested by Hartwig and Hall [45]. The viability of the high spin solution was tested through additional broken symmetry (BS) calculations at the converged high spin structures. All related computations were performed using Orca (Version 6.0.1) [46]. Geometry optimisations were performed using M06L/Def2-SVP/SMD [32,33,36] and single point broken symmetry computations at the M06/Def2-TZVP/SMD [32,33,36] level of theory. In all cases where self consistent field (SCF) convergence of the BS solution could be achieved, the ferromagnetic high spin solution was found to be at least equally stable.

**NMR.** NMR spectra for transition metal complexes were modelled using Orca (version 6.0.1) [46] and computed using the cmN15-L [47] functional. For the initial geometry optimisation, a Def2-SVP [33] basis set was used while the pcSseg-1 [48] basis set was used to model NMR spectra. Solvent effects were included through the SMD [36] implicit solvation model with parametrisation for acetonitrile. Computed chemical shifts were offset to tetramethylsilane (TMS) using experimental data for ferrocene [49] (4.15 ppm vs. TMS).

**Mechanistic Studies.** To gain insight into the mechanism of the reduction electron transfer (ET) potentials were calculated using DFT for the complex. In addition, the effect of ligand exchange, i.e. substitution of chloride with a solvent acetonitrile molecule, was investigated seeing that this was observed by Porta et al [29] in methanol solution. As a result, reduction potentials and Gibbs free energies were calculated for a set of the complex on the form  $[Fe_2Cl_x(MeCN)_{4-x}L]^{Y-X}$  where  $0 \leq X \leq 4$  is the number of chloride ligands and  $-1 \leq Y \leq +5$  is the total charge of the complex.

For the ligand exchange the reaction was divided into two steps: loss of chloride (Reaction 1) and the subsequent binding of acetonitrile (Reaction 2)).



Using the obtained Gibbs free energy values, the Gibbs free energy change for Reaction 1,  $\Delta G_1$ , and Reaction 2,  $\Delta G_2$ , were calculated. In addition, the loss of chloride was assumed to be the rate determining step and as such the activation energies for Reaction 1,  $\Delta G_1^\ddagger$ , were estimated using the method suggested by Hartwig and Hall [45].

Since no chloride ions were introduced to the experiment apart from those included in the complex, the chloride concentration in solution was assumed to be very low, effectively rendering Reaction 1 to be fully irreversible.

**Simulation.** The voltammetric behaviour was simulated using the DigiElch software supplied by Gamry. Potentials resulting from DFT calculations were used in the simulations, while the currents were based on the experimental value and known values of the electrode area and the complex concentration. The diffusion coefficients were set to the same value for the different complexes.

For the reversible couple, the heterogeneous rate constant was determined using a range of sweep rates from 0.02 to 2 Vs<sup>-1</sup>. In the simulation, a manual fit to one sweep rate was used to determine the parameters and these were used for all sweep rates.

For the entire voltammogram, electrochemical and chemical reaction steps were included. From the DFT calculations, the rate of the chemical reactions was estimated by using the activation enthalpy for the loss of chlorides. The electron transfer rates were set to the same value as for the reversible couple with exception of the first reduction of the bridged complex that was considered to be slow based on the experimental results.

### 3. Results and discussion

#### 3.1. Cyclic voltammetry

Cyclic voltammetry measurements of the complex in acetonitrile, Fig. 2a, showed a single reversible process at  $-0.29$  V vs. Ag/Ag<sup>+</sup> and a series of irreversible reduction peaks, with the most prominent showing at  $-0.84$ ,  $-1.3$ ,  $-1.5$ ,  $-1.9$ , and  $-2.2$  V vs. Ag/Ag<sup>+</sup>. The peak separation for the reversible redox process at  $-0.29$  V increases slightly with increasing sweep rate, indicating a fast quasi-reversible electron transfer, Fig. 2b In addition, the peak is unaffected by scans going as low as  $-2.5$  V vs. Ag/Ag<sup>+</sup> (Figure S1) despite the presence of irreversible reduction peaks. This is a clear sign that there is more than one form of the complex present in solution, where one gives rise to the reversible process while the other(s) are irreversibly reduced. The absence of an initialisation period [13,14] together with comparable measurements in methanol [29] suggest that the reversible peak is not the result of another iron species formed through decomposition but can indeed be associated with the Fe dimer complex.

This is in line with our earlier work [29] which suggests that the complex can be present in a bridged and a non-bridged form (Fig. 1) which are connected by a rather low barrier.

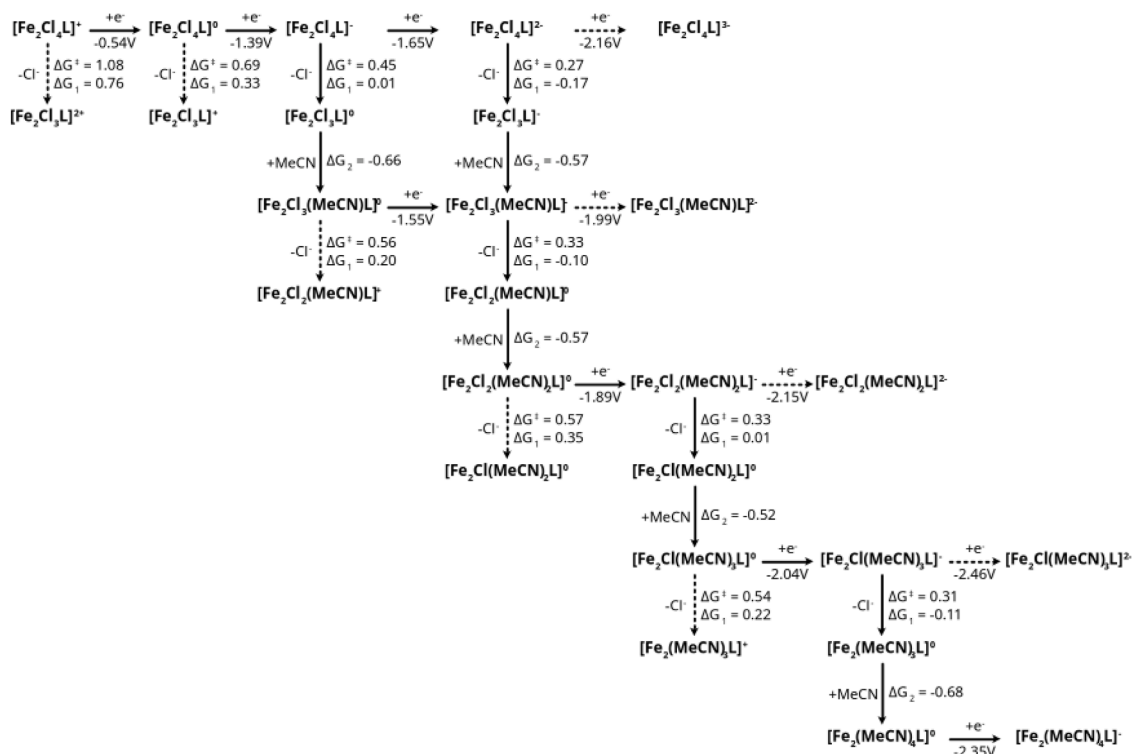


Fig. 3. Reaction pathway for the bridged complex. Horizontal arrows show reductions with potentials given in V vs. Ag/Ag<sup>+</sup>, and vertical arrows indicating ligand exchange by loss of chloride and addition of an acetonitrile with ΔG and ΔG<sup>‡</sup> given in eV. Dotted arrows indicate reactions that will not readily take place. The complete scheme is provided in the SI, Figure S7.

A similar equilibrium is also observed in acetonitrile (Figure S2). Both forms are roughly equally stable, especially in an interval between a total charge of 0 and -2. For positively charged complexes the bridged form is generally more stable while for negatively charged species with a charge of -3 or lower, the non-bridged is more stable. These results hold regardless of the number of bound chlorides (Table S1). Minima for the non-bridged {FeCl<sub>2</sub>}<sub>2</sub> and the bridged {Fe(Cl)(μ-Cl)<sub>2</sub>Fe(Cl)} forms are found at dihedral angles of 40° and 130°, respectively (see SI, Figure S2). Furthermore, a potential energy surface (PES) scan along the rotation dihedral suggests only a small to moderate yet long anharmonic barrier which spreads over a dihedral range of 90° between both isomers. Thus, an interconversion should, contrary to experimental evidence provided by the almost perfect reversibility of the first reduction peak, be unavoidable. This points towards a secondary effect not included in our simple solution phase model. In the absence of any direct indications for the underlying effect which stabilises either form, we can only speculate. One hypothesis is, that the very broad, anharmonic potential barrier between both minima (SI, Figure S2) results in a significant reduction of the overall isomerisation rate. Within the framework of the Grote-Hynes model, a broad barrier corresponds to a longer residence time in the transition state region and thus, a lower transmission coefficient [50, 51]. A transmission coefficient below one in turn reduces the frequency factor in the rate equation and thus, reduces the overall reaction rate in addition to any effects from the barrier height. Following earlier studies, a frequency factor far below one and thus, a significant reduction in the reaction rate can be expected for the broad, anharmonic barrier associated with the interconversion between bridged and non-bridged form [52].

### 3.2. NMR

In an attempt to gain insights into the oxidation state of the iron centra and the present isomers in solution, <sup>1</sup>HNMR spectra were collected for a 1 mM solution of the complex in acetonitrile-d<sub>3</sub>, at both

25 °C and 50 °C, Figure S3. This method has previously been employed by Porta et al. for the same complex in methanol solution [29] where a paramagnetic shift was observed indicating the presence of high spin iron(II) in the complex. Furthermore, DFT modelling of the NMR spectra might behave differently for the two isomers. However, measured <sup>1</sup>HNMR spectra in acetonitrile possess no paramagnetic shift at either temperature. This is also confirmed by DFT calculations which suggests a strong influence of the solvent on the presence of a paramagnetic shift. In light of the error bars associated with computed NMR spectra [53] and the overall complexity of the experimental data we refrained from a more detailed comparison. Overall, these results show, that it is not possible to discern the two isomers using standard spectroscopic techniques. Accordingly, we have to rely on DFT modelling to obtain insights into the speciation and potential mechanisms resulting in the reversibility and irreversibility of the observed reduction peaks in the CV.

### 3.3. Bridged complex

Experiments suggest that at least two independent species must be present to explain the observed CV. Following the discussion above, the most likely candidates are the complex in its bridged and non-bridged form. Let us start the discussion with the redox behaviour of the bridged complex. Following the above discussion, we will neglect the possibility for isomerisation and focus solely on possible reduction steps and the possibility of Cl<sup>-</sup> release or exchange by acetonitrile which would result in an irreversible reaction.

The reaction cycle starts with a positively charged [Fe<sub>2</sub>Cl<sub>4</sub>]<sup>+</sup> species which is present under open circuit conditions and proceeds through two reduction steps at potentials of -0.54 V and -1.39 V vs. Ag/Ag<sup>+</sup>. While the second potential corresponds well to the observed peak at -1.3 V vs. Ag/Ag<sup>+</sup>, the -0.54 V does not correspond to neither the reversible peak at -0.29 V, nor the -0.84 V peak. From a thermodynamic point of view, chloride release is endergonic at both the intermediate and the reactant and subject to a moderate to high activation

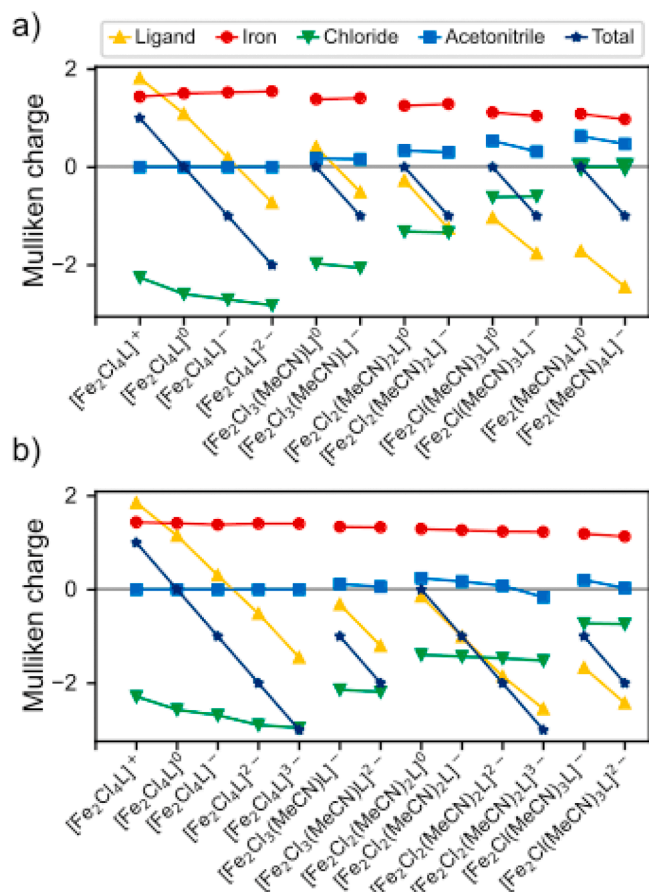


**Fig. 4.** Charges from Mulliken population analysis for the a) bridged and b) non-bridged complex with the sum of Mulliken assigned charges for the different parts of the complex for all species that are part of the suggested reaction path in Fig. 3 and 6 respectively. Points connected with lines indicate electron transfers for a set number of chloride ions. Detailed distributions are provided in the SI, Figures S9 to S17.

barrier which effectively blocks this reaction (Fig. 3). Thus, at least the first reduction step should be reversible, as shown in Fig. 5 where no kinetics are involved. The assignment of this peak is further discussed in relation to the non-bridged complex. Surprisingly, the electrons added to the system do not result in a reduction of the Fe centres but are instead symmetrically placed at the Cl and <sup>Me</sup>bppi ligand (Fig. 4 and SI, Figure S9a). Thus, the reduction reactions are fully ligand centred and the metal only acts as a spectator. Naturally, an increased negative charge at the Cl<sup>-</sup> ligands makes their release thermodynamically and kinetically more favourable which is indeed seen in our computations (Fig. 3).

Following the second reduction, Cl<sup>-</sup> exchange by acetonitrile starts to become thermodynamically favourable. The ligand exchange occurs through a two-step process whereby Cl<sup>-</sup> is released in the first step resulting in a free coordination site which is then filled by acetonitrile. The initial chloride release is thermoneutral, i.e. the change in Gibbs free energy is approximately 0.0 eV. This is then followed by a strongly exergonic coordination of acetonitrile to the Fe centre. The overall reaction is, despite these favourable thermodynamics still rather slow owing to a moderate activation barrier of 0.45 eV for the initial chloride release. The release of a second Cl<sup>-</sup> is even less likely owing to a slightly endergonic reaction and an even higher barrier of 0.56 eV (Fig. 3). Assuming the ligand release takes place, the reduction will require a potential of -1.55 V vs. Ag/Ag<sup>+</sup>. Both this and the previous reduction steps are, owing to the release of a Cl<sup>-</sup> ligand irreversible. Following this ligand change, the charge distribution starts to display an asymmetry at

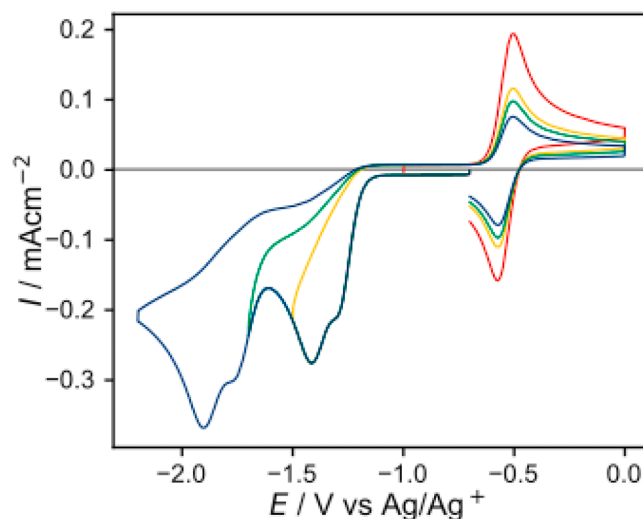


**Fig. 5.** Simulated cyclic voltammograms for the bridged complex according to Fig. 3 but limited to the potential range used experimentally. Sweep rate 0.1 Vs<sup>-1</sup>.

the Fe centre, i.e. the Fe atom at which the ligand exchange occurred has a slightly less positive charge of 0.65e compared to 0.73e for the other Fe centre (see SI, Figure S10a). This asymmetry becomes even more pronounced for the subsequent ligand centered electron transfer step during which the electron is almost exclusively placed at one half of the organic ligand (see Fig. 4 and SI, Figure S10a and S10b).

An alternative to the ligand exchange is the direct reduction of the complex which occurs at a slightly more negative potential of -1.65 V vs. Ag/Ag<sup>+</sup> (see Fig. 3). The additional electron is, identical to the preceding two reduction steps again symmetrically placed on the organic ligand while only a negligible change in charge density is observed at the Fe centres. Following this reduction, substitution of Cl<sup>-</sup> by acetonitrile is thermodynamically feasible and subject to only a minor barrier of 0.27 eV (Fig. 3). Following this ligand exchange, both reaction routes merge again. The competing fourth reduction is with a potential of -2.16 V vs. Ag/Ag<sup>+</sup> not yet possible.

Experimentally, an irreversible reduction peak is observed at -1.5 V which agrees well with the predictions made by either reaction path.

Following this sequence of reductions and ligand exchange processes, a second Cl<sup>-</sup> ligand is replaced by acetonitrile. This reaction is subject to a low barrier of 0.33 eV and both the ligand release, and the coordination of acetonitrile are exergonic (Fig. 3). The competing fourth reduction step is with a potential of -1.99 V vs. Ag/Ag<sup>+</sup> still not yet possible under reaction conditions. The resulting complex possesses again a symmetric ligand distribution which in turn also renders the charge distribution symmetric (see SI, Figure S16a).

The subsequent reduction then requires a potential of -1.89 V vs. Ag/Ag<sup>+</sup> and is followed by replacing a bridging chloride ligand through a third acetonitrile. This matches again well with the experimentally observed peak at -1.9 V. This step is subject to only a minor barrier of 0.33 eV and slightly exergonic. It is remarkable that even this fourth electron is placed symmetrically on the ligand with almost no variation of the electron density at the Fe centres. Moving towards even more negative potentials in the CV measurement, a fifth reduction at a potential of -2.04 V vs. Ag/Ag<sup>+</sup> directly followed by an exergonic exchange of the last Cl<sup>-</sup> ligand becomes possible. This reaction can again be mapped to an experimentally observed peak at -2.2 V in the CV measurement (Figure S1).

Since this is a zero-chlorido complex, no further ligand exchange is possible, instead it is predicted to be reduced at -2.35 V. This potential lies outside of the potential window considered in the CVs in Fig. 2.

Simulation of the voltammetry for the bridged complex according to

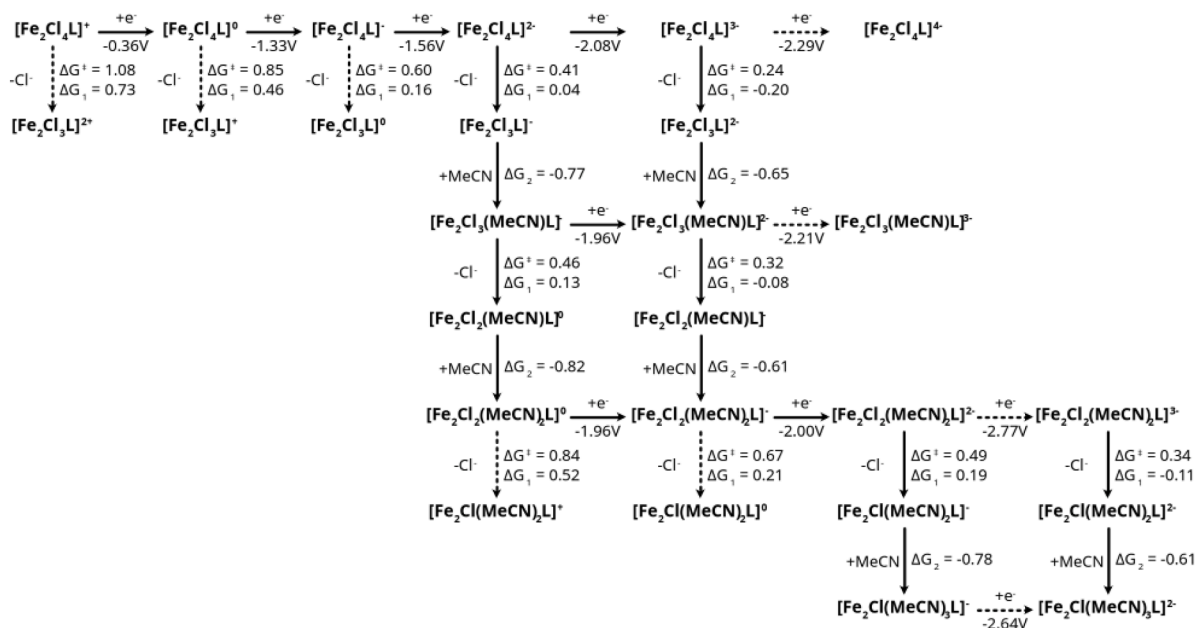


Fig. 6. Reaction pathway for the non-bridged complex. Horizontal arrows show reductions with potentials given in V vs. Ag/Ag<sup>+</sup>, and vertical arrows indicate ligand exchange by loss of chloride and addition of an acetonitrile with ΔG and ΔG<sup>‡</sup> given in eV. Dotted arrows indicate reactions that will not readily take place. The complete scheme is provided in the SI, Figure S8.

Fig. 3 is shown in Fig. 5. The heterogeneous rate constants are the same for all electron transfers reactions involved.

Overall, reduction steps of the bridged complex tend to be coupled with a ligand exchange which renders these steps irreversible. Indeed, most of the computed potentials match reasonably well with the irreversible peaks observed in the CV, Fig. 2a. It is therefore reasonable to assume that the irreversible reduction steps observed in the CV belong to the bridged complex. However, it can clearly not account for the reversible reduction since the only potentially reversible peak at -0.54 V is too far away from the measured potential of -0.29 V. In addition, the peak observed at -0.84 V is missing in the reaction path. This gives further support for the hypothesis that there is more than one form of the complex present in acetonitrile solution even at OCP.

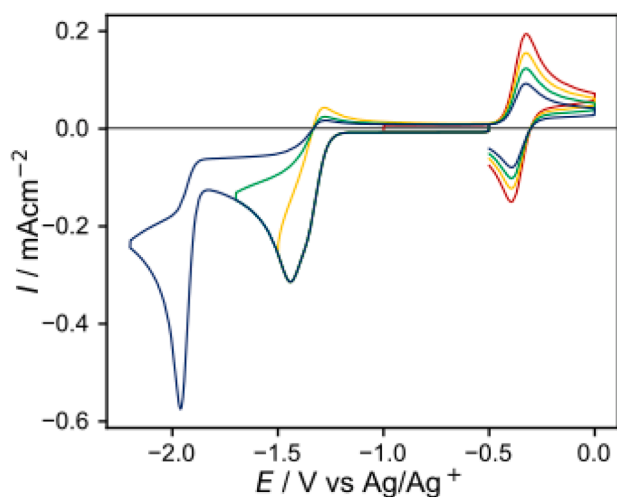


Fig. 7. Simulated cyclic voltammograms for the non-bridged complex according to Fig. 6 but limited to the potential range used experimentally. Sweep rate 0.1 V s<sup>-1</sup>.

### 3.4. Non-Bridged complex

The predicted redox potentials and their irreversibility for the bridged complex provide an explanation for the majority of the irreversible peaks in the CV. However, this system completely fails to explain the presence of a persistent reversible redox reaction at -0.29 V vs. Ag/Ag<sup>+</sup> (Figs. 2 and 5). We therefore performed an identical analysis for the non-bridged complex.

Just as for the bridged complex, the reaction starts with the four-chloride complex [Fe<sub>2</sub>Cl<sub>4</sub>L]<sup>+</sup>. Ligand exchange is blocked by a very high barrier of 1.08 eV (see Fig. 6). Instead, the complex undergoes successive reduction to [Fe<sub>2</sub>Cl<sub>4</sub>L]<sup>0</sup> (ΔG<sup>‡</sup> = 0.85 eV) at -0.36 V, [Fe<sub>2</sub>Cl<sub>4</sub>L]<sup>-</sup> (ΔG<sup>‡</sup> = 0.60 eV) at -1.33 V, and finally to [Fe<sub>2</sub>Cl<sub>4</sub>L]<sup>2-</sup> at -1.56 V. Ligand release at the first two intermediates is again blocked by moderate to high barriers of 0.85 eV and 0.60 eV, respectively.

From [Fe<sub>2</sub>Cl<sub>4</sub>L]<sup>2-</sup> two paths are possible. The first path starts with a reduction at -2.08 V to [Fe<sub>2</sub>Cl<sub>4</sub>L]<sup>3-</sup>, which then undergoes 2 fast ligand exchanges that are both exergonic and subject to only minor barriers of 0.24 eV and 0.32 eV. Reduction of the tetrachlorido and trichlorido diiron intermediates is not possible under the applied potential since they require potentials of approximately -2.2 V which lies outside the measurement range.

Alternatively, the ligand exchange from [Fe<sub>2</sub>Cl<sub>4</sub>L]<sup>2-</sup> to [Fe<sub>2</sub>Cl<sub>3</sub>(MeCN)L]<sup>-</sup> occurs prior to reduction. Both reaction steps involved in the ligand exchange are either thermoneutral or exergonic and overall only subject to a moderate barrier of 0.41 eV. Once the ligand has been exchanged, the complex can be reduced at a slightly less negative potential of -1.96 V or facilitate an additional ligand exchange. The initial Cl<sup>-</sup> release is slightly endergonic by 0.13 eV and subject to a moderate barrier of 0.46 eV and is therefore in principle possible. Interestingly, this additional ligand exchange does not affect the redox potential further, i.e. it still requires a potential of -1.9 V.

Seeing that the experimentally observed peak lies closer to -1.9 than -2.0 V, while -2.29 and -2.21 V lies outside of the experimental voltage range, it is likely that the reaction proceeds through, either single or double, initial ligand exchange, resulting in reduction at -1.96 V rather than -2.08 V. However considering the errors in the calculated values this cannot be said for certain.

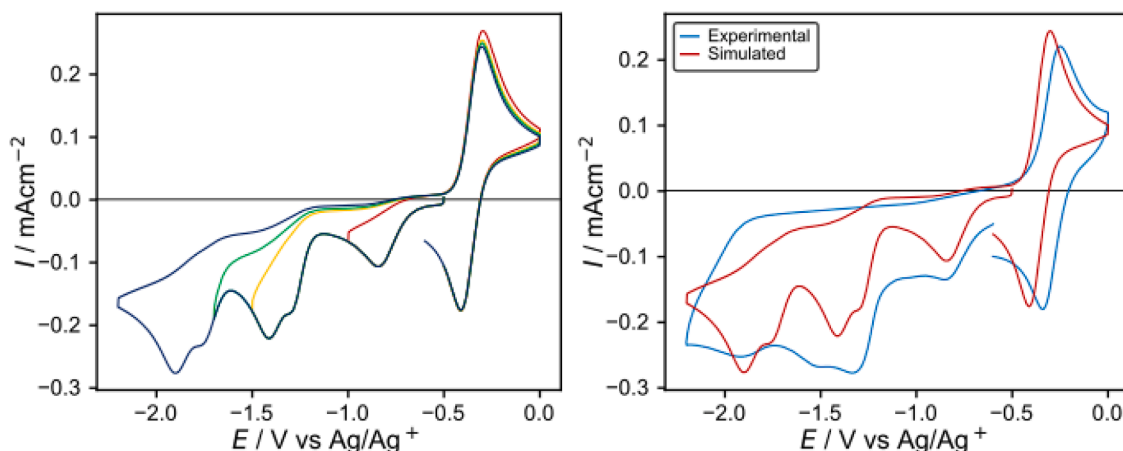


**Fig. 8.** Simulated cyclic voltammograms for the bridged complex in equilibrium with the non-bridged complex. For the non-bridged complex, only the electron transfer at  $-0.36$  V vs. Ag/AgCl is involved (left). Comparison between experimental (blue) and simulated (red) voltammograms at  $0.1$  Vs $^{-1}$  (right).

Under the applied potential, the formed dichlorido diiron complex is subject to an immediate second reduction which requires a slightly lower potential of  $-2.00$  V vs. Ag/Ag $^{+}$ .

Of these reductions, only the fully reversible peak at  $-0.36$  V vs. Ag/Ag $^{+}$  matches with the experimentally observed peak at  $-0.29$  V. All other reductions fall into the range where exclusively irreversible peaks are observed (see Fig. 6). The absence of any additional fully reversible peaks together with the robustness of the redox reaction at  $-0.29$  V vs. Ag/Ag $^{+}$  suggests that an additional mechanism is present which inhibits the subsequent reduction steps. Unfortunately, neither computations nor experiments provide any hints at the nature of this mechanism.

Identical to the bridged complex, again no significant charge transfer to the metal centres is observed upon reduction. Instead, the electrons are again exclusively placed at the organic ligand and distributed symmetrically between both halves. Identical behaviour is also observed for all other reduction steps of symmetric ligand structures, i.e. they are ligand centred and symmetrically distributed on both fragments. Identical to the bridged complex, deviations corresponding to an asymmetric charge distribution are only observed for asymmetric ligand distributions.

Simulation of the voltammetry for the non-bridged complex according to Fig. 6 is shown in Fig. 7. As for the bridged complex, the heterogeneous rate constants are the same for all electron transfer reactions involved.

The predicted potential of  $-0.36$  V vs. Ag/Ag $^{+}$  for the first ET corresponds well to the observed potential of  $-0.29$  V, however, the suggested mechanism fails to explain the consistent peak currents of the process at  $-0.29$  V, Fig. 2, and some reversibility is observed for the process at  $-1.33$  V in contrast to the experiment. In addition, the processes at  $-1.33$ ,  $-1.56$ , and  $-2.08$  V are not well separated and the two processes at  $-1.96$  V give rise to a large current which is not found in the experiment. This demonstrates the non-bridged complex is not reduced at potentials more negative than the standard potential at  $-0.29$  V vs. Ag/AgCl.

Also, for the non-bridged complex, the peak at  $-0.84$  V is missing. Since the bridged complex is favoured for the  $[\text{Fe}_2\text{Cl}_4\text{L}]^+$  complex by  $0.25$  eV according to the DFT calculation, simulations were made starting with only the bridged complex but with an equilibrium between  $[\text{Fe}_2\text{Cl}_4\text{L}]^+$  for the bridged complex with  $[\text{Fe}_2\text{Cl}_4\text{L}]^0$  of the non-bridged complex. The irreversible peak at  $-0.84$  V was used to change the concentration and the rate of the first electron transfer for the bridged compound,  $[\text{Fe}_2\text{Cl}_4\text{L}]^+ / [\text{Fe}_2\text{Cl}_4\text{L}]^0$ . Instead of a rate constant of  $0.1$  cm $^{-1}$ , a quasi-reversible electron transfer with rate constant  $2 \cdot 10^{-5}$  cm $^{-1}$  was required. For the rest of the electron transfer reactions the rate was the same as in previous simulations. The result is shown left in Fig. 8. All experimental peaks are represented in the simulation and the

reversibility of the peak at  $-0.29$  V is preserved, right in Fig. 8.

The main difference is the resolution of the peaks, where the experiment has broader peaks, probably due to adsorption on the glassy carbon electrode. For the voltammograms in Fig. 2, the same electrode was used in a sequence without polishing the electrode in between and as noted before this may influence the response.

Regardless, the fact that a qualitative agreement between the experimental result and DFT calculations is established indicates that the reaction mechanisms proposed describe the electrochemical behaviour of the complex in a comprehensive way. The most important electrochemical result is the very stable redox reaction at  $-0.29$  V vs. Ag/Ag $^{+}$ , which potentially could be used for redox catalysis. From the DFT calculation, it was also concluded that the electrochemical behaviour is ligand based, i.e. the iron centres in the complex are not directly involved in the processes.

#### 4. Conclusions

We performed a detailed electrochemical analysis of a rotationally flexible Fe dimer embedded into a  $\text{Me}^{\text{b}}\text{ppbbi}$  ligand system. CV measurements indicate the presence of a fully reversible peak at  $-0.29$  V which could be used for electrocatalysis. This peak is associated with the non-bridged form of the complex. The bridged form on the other hand undergoes stepwise Cl $^{-}$  ligand exchange with acetonitrile. This renders its reduction irreversible and thus, the closed form potentially unsuitable as electrocatalyst. Thus, more research is needed to identify ways to stabilise the catalyst before this ligand system can be used as electrocatalyst. Surprisingly, all reductions are ligand centred which highlights the ability of this organic ligand to store multiple electrons and thus, suggests that the metal is not necessarily involved in the electrochemical reduction or oxidation steps if an extended  $\pi$  electron system is present.

#### Declaration of competing interest

The authors declare the following financial interests/personal relationships which may be considered as potential competing interests: Michael Busch reports financial support was provided by Knut and Alice Wallenberg Foundation. If there are other authors, they declare that they have no known competing financial interests or personal relationships that could have appeared to influence the work reported in this paper.

#### Acknowledgements

M.B. acknowledges financial support through the Wallenberg Initiative Materials Science for Sustainability (WISE) funded by the Knut and Alice Wallenberg foundation. The Swedish NMR Centre is

acknowledged for help with the NMR spectra. Computational resources were provided by the National Academic Infrastructure for Supercomputing in Sweden (NAISS) through grants NAISS 2023/5-538, NAISS 2024/5-310, and NAISS 2025/5-365.

## Supplementary materials

Supplementary material associated with this article can be found, in the online version, at [doi:10.1016/j.electacta.2026.149122](https://doi.org/10.1016/j.electacta.2026.149122).

## References

- [1] C. Elschenbroich, *Organometallics*, 3rd ed., Wiley-VCH, Weinheim, 2006.
- [2] S.B. Rubashkin, M.-T. Nguyen, Y. Chen, D. Malhotra, A.M. Appel, E.S. Wiedner, Electrocatalysis in CO<sub>2</sub>-binding organic liquids with an iron porphyrin, *ACS Electrochem.* 1 (2025) 689–698, <https://doi.org/10.1021/acselectrochem.4c00170>.
- [3] R. Khakpour, D. Lindberg, K. Laasonen, M. Busch, CO<sub>2</sub> or carbonates – What is the active species in electrochemical CO<sub>2</sub> reduction over Fe-porphyrin? *ChemCatChem* 15 (2023) e202201671 <https://doi.org/10.1002/cctc.202201671>.
- [4] A. Singh, A. Zamader, R. Khakpour, K. Laasonen, M. Busch, M. Robert, Molecular electrochemical catalysis of CO-to-formaldehyde conversion with a cobalt complex, *J. Am. Chem. Soc.* 146 (2024) 22129–22133, <https://doi.org/10.1021/jacs.4c06878>.
- [5] R. Khakpour, K. Farshadfar, S.-T. Dong, B. Lassalle-Kaiser, K. Laasonen, M. Busch, Mechanism of CO<sub>2</sub> electroreduction to multicarbon products over iron phthalocyanine single-atom catalysts, *J. Phys. Chem. C* 128 (2024) 5867–5877, <https://doi.org/10.1021/acs.jpcc.3c08347>.
- [6] Q. Zhu, C.L. Rooney, H. Shema, C. Zeng, J.A. Panetier, E. Gross, H. Wang, L. R. Baker, The solvation environment of molecularly dispersed cobalt phthalocyanine determines methanol selectivity during electrocatalytic CO<sub>2</sub> reduction, *Nat. Catal.* 7 (2024) 987–999, <https://doi.org/10.1038/s41929-024-01190-9>.
- [7] S. Amthor, D. Hernández-Castillo, B. Maryasin, P. Seeber, A.K. Mengele, S. Gräfe, L. González, S. Rau, Strong Ligand stabilization based on  $\pi$ -extension in a series of ruthenium terpyridine water oxidation catalysts, *Chem. - Eur. J.* 27 (2021) 16871–16878, <https://doi.org/10.1002/chem.202102905>.
- [8] Y. Liou, S.-M. Ng, S.-M. Yiu, W.W.Y. Lam, S.-G. Wei, K.-C. Lau, T.-C. Lau, Catalytic water oxidation by ruthenium(II) quaterpyridine (qpy) complexes: evidence for ruthenium(III) qpy-N<sup>III</sup>-dioxide as the real catalysts, *Angew. Chem., Int. Ed.* 53 (2014) 14468–14471, <https://doi.org/10.1002/anie.201408795>.
- [9] S.W. Gersten, G.J. Samuels, T.J. Meyer, Catalytic oxidation of water by an oxo-bridged ruthenium dimer, *J. Am. Chem. Soc.* 104 (1982) 4029–4030.
- [10] A.D. Cypcar, K.M. Bui, J.Y. Yang, Suppressing H<sub>2</sub> evolution with sterically encumbered proton sources to improve the faradaic efficiency for CO<sub>2</sub> reduction to formate, *ACS Catal.* 14 (2024) 14517–14523, <https://doi.org/10.1021/acscatal.4c03809>.
- [11] T.S. Lobana, Recent trends in bonding and structure of metal derivatives of phosphine chalcogenides, *Discov. Chem.* 2 (2025) 67, <https://doi.org/10.1007/s44371-025-00131-0>.
- [12] G.R.F. Orton, B.S. Pilgrim, N.R. Champness, The chemistry of phosphines in constrained, well-defined microenvironments, *Chem. Soc. Rev.* 50 (2021) 4411–4431, <https://doi.org/10.1039/D0CS01556C>.
- [13] K.J. Lee, B.D. McCarthy, J.L. Dempsey, On decomposition, degradation, and voltammetric deviation: the electrochemist's field guide to identifying precatalyst transformation, *Chem. Soc. Rev.* 48 (2019) 2927–2945, <https://doi.org/10.1039/C8CS00851E>.
- [14] J. Li, C.A. Triana, W. Wan, D.P. Adiyeri Saseendran, Y. Zhao, S.E. Balaghi, S. Heidari, G.R. Patzke, Molecular and heterogeneous water oxidation catalysts: recent progress and joint perspectives, *Chem. Soc. Rev.* 50 (2021) 2444–2485, <https://doi.org/10.1039/D0CS00978D>.
- [15] M.N. Hossain, R. Khakpour, M. Busch, M. Suominen, K. Laasonen, T. Kallio, Temperature-controlled syngas production via electrochemical CO<sub>2</sub> reduction on a CoTPP/MWCNT composite in a flow cell, *ACS Appl. Energy Mater.* 6 (2023) 267–277, <https://doi.org/10.1021/acsaem.2c02873>.
- [16] C. Cometto, L. Chen, D. Mendoza, B. Lassalle-Kaiser, T.-C. Lau, M. Robert, An iron quaterpyridine complex as precursor for the electrocatalytic reduction of CO<sub>2</sub> to methane, *ChemSusChem* 12 (2019) 4500–4505, <https://doi.org/10.1002/cssc.201902040>.
- [17] S.-T. Dong, C. Xu, B. Lassalle-Kaiser, Multiple C–C bond formation upon electrocatalytic reduction of CO<sub>2</sub> by an iron-based molecular macrocycle, *Chem. Sci.* 14 (2023) 550–556, <https://doi.org/10.1039/D2SC04729B>.
- [18] H. Nishihara, K. Pressprich, R.W. Murray, J.P. Collman, Electrochemical olefin epoxidation with manganese meso-tetraphenylporphyrin catalyst and hydrogen peroxide generation at polymer-coated electrodes, *Inorg. Chem.* 29 (1990) 1000–1006, <https://doi.org/10.1021/ic000330a020>.
- [19] H. Wu, Y. Xu, P. Guo, Y. Xu, Z. Huang, L. Zhang, Electrochemical epoxidation of alkene with high faradaic efficiencies using water as an oxygen source, *Green. Chem.* 26 (2024) 2922–2927, <https://doi.org/10.1039/D3GC05126A>.
- [20] R.A. Binstead, C.W. Chronister, J. Ni, C.M. Hartshorn, T.J. Meyer, Mechanism of water oxidation by the  $\mu$ -oxo dimer [(bpy)<sub>2</sub>(H<sub>2</sub>O)RuIIORuII(OH<sub>2</sub>)(bpy)<sub>2</sub>]<sup>4+</sup>, *J. Am. Chem. Soc.* 122 (2000) 8464–8473, <https://doi.org/10.1021/ja993235n>.
- [21] M. Gil-Sepulcre, A. Llobet, Molecular water oxidation catalysts based on first-row transition metal complexes, *Nat. Catal.* 5 (2022) 79–82.
- [22] J. Campos, Bimetallic cooperation across the periodic table, *Nat. Rev. Chem.* 4 (2020) 696–702, <https://doi.org/10.1038/s41570-020-00226-5>.
- [23] G. Li, D. Zhu, X. Wang, Z. Su, M.R. Bryce, Dinuclear metal complexes: multifunctional properties and applications, *Chem. Soc. Rev.* 49 (2020) 765–838, <https://doi.org/10.1039/C8CS00660A>.
- [24] I.G. Powers, C. Uyeda, Metal–metal bonds in catalysis, *ACS Catal.* 7 (2017) 936–958, <https://doi.org/10.1021/acscatal.6b02692>.
- [25] B.J. Wallar, J.D. Lipscomb, Dioxxygen activation by enzymes containing binuclear non-heme iron clusters | chemical reviews, *Chem. Rev.* 96 (1996) 2625–2658, <https://doi.org/10.1021/cr9500489>.
- [26] L. Que, W.B. Tolman, Biologically inspired oxidation catalysis, *Nature* 455 (2008) 333–340, <https://doi.org/10.1038/nature07371>.
- [27] W. Kang, C.C. Lee, A.J. Jasniowski, M.W. Ribbe, Y. Hu, Structural evidence for a dynamic metallocofactor during N<sub>2</sub> reduction by mo-nitrogenase, *Science* (1979) 368 (2020) 1381–1385, <https://doi.org/10.1126/science.aaz6748>.
- [28] E. Muller, G. Bernardinelli, J. Reedijk, 4,4'-Bis(2-picolinimino)-2,2'-bibenzimidazoles: a new class of dinucleating ligands which allow for a tuning of the metal-metal distance. structures and properties of a dicopper(II) complex and of two oxygenation products of a dicopper(I) complex; a tentative coordination chemical modeling of hemocyanin, *Inorg. Chem.* 34 (1995) 5979–5988, <https://doi.org/10.1021/ic00128a008>.
- [29] P.G. Porta, B. Kintzel, B. Weber, M. Busch, D. Sorsche, Entropy-driven ligand exchange in a rotationally flexible dinuclear Fe(II)-Fe(II) complex, *ChemRxiv* (2025), <https://doi.org/10.26434/chemrxiv-2025-gchml> n.d.
- [30] G. Gritzner, Standard electrode potentials of M+M couples in non-aqueous solvents (molecular liquids), *J. Mol. Liq.* 156 (2010) 103–108, <https://doi.org/10.1016/j.molliq.2010.03.010>.
- [31] M.J. Frisch, G.W. Trucks, H.B. Schlegel, G.E. Scuseria, M.A. Robb, J.R. Cheeseman, G. Scalmani, V. Barone, G.A. Petersson, H. Nakatsuji, X. Li, M. Caricato, A. V. Marenich, J. Bloino, B.G. Janesko, R. Gomperts, B. Mennucci, H.P. Hratchian, J. V. Ortiz, A.F. Izmaylov, J.L. Sonnenberg, D. Williams-Young, F. Ding, F. Lipparini, F. Egidi, J. Goings, B. Peng, A. Petrone, T. Henderson, D. Ranasinghe, V. G. Zakrzewski, J. Gao, N. Rega, G. Zheng, W. Liang, M. Hada, M. Ehara, K. Toyota, R. Fukuda, J. Hasegawa, M. Ishida, T. Nakajima, Y. Honda, O. Kitao, H. Nakai, T. Vreven, K. Throssell, J.A. Montgomery Jr., J.E. Peralta, F. Ogliaro, M. J. Bearpark, J.J. Heyd, E.N. Brothers, K.N. Kudin, V.N. Staroverov, T.A. Keith, R. Kobayashi, J. Normand, K. Raghavachari, A.P. Rendell, J.C. Burant, S.S. Iyengar, J. Tomasi, M. Cossi, J.M. Millam, M. Klene, C. Adamo, R. Cammi, J.W. Ochterski, R.L. Martin, K. Morokuma, O. Farkas, J.B. Foresman, D.J. Fox, *Gaussian 16 Revision C.01*, 2016.
- [32] Y. Zhao, D.G. Truhlar, A new local density functional for main-group thermochemistry, transition metal bonding, thermochemical kinetics, and noncovalent interactions, *J. Chem. Phys.* 125 (2006) 194101, <https://doi.org/10.1063/1.2370993>.
- [33] F. Weigend, R. Ahlrichs, Balanced basis sets of split valence, triple zeta valence and quadruple zeta valence quality for H to Rn: design and assessment of accuracy, *Phys. Chem. Chem. Phys.* 7 (2005) 3297, <https://doi.org/10.1039/b508541a>.
- [34] B. Mennucci, R. Cammi, J. Tomasi, Excited states and solvatochromic shifts within a nonequilibrium solvation approach: a new formulation of the integral equation formalism method at the self-consistent field, configuration interaction, and multiconfiguration self-consistent field level, *J. Chem. Phys.* 109 (1998) 2798–2807, <https://doi.org/10.1063/1.476878>.
- [35] G. Scalmani, M.J. Frisch, Continuous surface charge polarizable continuum models of solvation. i. general formalism, *J. Chem. Phys.* 132 (2010) 114110, <https://doi.org/10.1063/1.3359469>.
- [36] A.V. Marenich, C.J. Cramer, D.G. Truhlar, Universal solvation model based on solute electron density and on a continuum model of the solvent defined by the bulk dielectric constant and atomic surface tensions, *J. Phys. Chem. B* 113 (2009) 6378–6396, <https://doi.org/10.1021/jp810292n>.
- [37] M. Sotoudeh, K. Laasonen, M. Busch, Benchmarking the computed proton solvation energy and absolute potential in non-aqueous solvents, *Electrochim. Acta* 443 (2023) 141785, <https://doi.org/10.1016/j.electacta.2022.141785>.
- [38] M. Busch, E. Ahlberg, E. Ahlberg, K. Laasonen, How to predict the pK<sub>a</sub> of any compound in any solvent, *ACS Omega* 7 (2022) 17369–17383, <https://doi.org/10.1021/acsomega.2c01393>.
- [39] J.M. Herbert, Dielectric continuum methods for quantum chemistry, *WIREs Comput. Mol. Sci.* 11 (2021) e1519, <https://doi.org/10.1002/wcms.1519>.
- [40] E.S. Böes, P.R. Livotto, H. Stassen, Solvation of monovalent anions in acetonitrile and N,N-dimethylformamide: parameterization of the IEF-PCM model, *Chem. Phys.* 331 (2006) 142–158, <https://doi.org/10.1016/j.chemphys.2006.08.028>.
- [41] R.F. Ribeiro, A.V. Marenich, C.J. Cramer, D.G. Truhlar, Use of solution-phase vibrational frequencies in continuum models for the free energy of solvation, *J. Phys. Chem. B* 115 (2011) 14556–14562, <https://doi.org/10.1021/jp205508z>.
- [42] NIST Chemistry WebBook. <https://webbook.nist.gov/chemistry/> (accessed. (Accessed 25 February 2026).
- [43] M. Busch, K. Laasonen, E. Ahlberg, Method for the accurate prediction of electron transfer potentials using an effective absolute potential, *Phys. Chem. Chem. Phys.* 22 (2020) 25833–25840, <https://doi.org/10.1039/D0CP04508J>.
- [44] D.R. Lide (Ed.), *CRC Handbook of Chemistry and Physics*, 85th ed., CRC Press, Boca Raton, 2004.
- [45] J.F. Hartwig, K.S. Cook, M. Hapke, C.D. Incarvito, Y. Fan, C.E. Webster, M.B. Hall, Rhodium boryl complexes in the catalytic, terminal functionalization of alkanes, *J. Am. Chem. Soc.* 127 (2005) 2538–2552, <https://doi.org/10.1021/ja045090c>.

- [46] F. Neese, Software update: the orca program system—version 6.0, *WIREs Comput. Mol. Sci.* 15 (2025) e70019, <https://doi.org/10.1002/wcms.70019>.
- [47] C.J. Schattenberg, M. Kaupp, Implementation and first evaluation of strong-correlation-corrected local hybrid functionals for the calculation of NMR shieldings and shifts, *J. Phys. Chem. A* 128 (2024) 2253–2271, <https://doi.org/10.1021/acs.jpca.3c08507>.
- [48] F. Jensen, Segmented contracted basis sets optimized for nuclear magnetic shielding, *J. Chem. Theory. Comput.* 11 (2015) 132–138, <https://doi.org/10.1021/ct5009526>.
- [49] M. Agnes, A. Nitti, D.A.V. Griend, D. Dondi, D. Merli, D. Pasini, A chiroptical molecular sensor for ferrocene, *Chem. Commun.* 52 (2016) 11492–11495, <https://doi.org/10.1039/C6CC05937F>.
- [50] R. Bianco, P.J. Hay, J.T. Hynes, Theoretical study of O O single bond formation in the oxidation of water by the ruthenium blue dimer, *J. Phys. Chem. A* 115 (2011) 8003–8016, <https://doi.org/10.1021/jp200309d>.
- [51] B.J. Gertner, K.R. Wilson, J.T. Hynes, Nonequilibrium solvation effects on reaction rates for model SN2 reactions in water, *J. Chem. Phys.* 90 (1989) 3537–3558, <https://doi.org/10.1063/1.455864>.
- [52] I.S. Tolokh, G.W.N. White, S. Goldman, C.G. Gray, Prediction of ion channel transport from grotte—hynes and kramers theories, *Mol. Phys.* 100 (14) (2002) 2351–2359.
- [53] C.J. Schattenberg, M. Kaupp, Extended benchmark set of main-group nuclear shielding constants and NMR chemical shifts and its use to evaluate modern DFT methods, *J. Chem. Theory. Comput.* 17 (2021) 7602–7621, <https://doi.org/10.1021/acs.jctc.1c00919>.